Journal of *Marine Science and Engineering*

MDPI

Article

Revisiting the Carbonate Chemistry of the Sea of Japan (East Sea): From Water Column to Sediment

Pavel Tishchenko [1,*], Jing Zhang [2], Galina Pavlova [1], Petr Tishchenko [1], Sergey Sagalaev [1] and Mariya Shvetsova [1]

[1] V.I. Il'ichev Pacific Oceanological Institute, Far Eastern Branch, Russian Academy of Sciences, 690041 Vladivostok, Russia; pavlova@poi.dvo.ru (G.P.); eq15@poi.dvo.ru (P.T.); sagalaev@poi.dvo.ru (S.S.); chippers@rambler.ru (M.S.)

[2] Faculty of Science, University of Toyama, 3190 Gofuku, Toyama 930-8555, Toyama, Japan; jzhang@sci.u-toyama.ac.jp

* Correspondence: tpavel@poi.dvo.ru; Tel.: +7-423-231-3092

Abstract: In this study, we investigated the carbonate system in sediments and water columns from five stations in the Sea of Japan (East Sea) (JES) during the R/V Hakuho Maru KH-10-2 research cruise in the summer of 2010. The total alkalinity (TA) and pH were measured. Adopting a saturation degree of 91% and 80% for the lysocline depth and calcite compensation depth (CCD), respectively, we found that those depths corresponded to 1360 and 1980 m. A comparison of the calcite saturation depths, lysocline depths, and CCD depths obtained for 1999 and 2010 suggests that acidification of the interior of the JES occurred. Sediment cores were retrieved using a multi-corer. In the sediment cores, a sharp decrease in the pH by 0.3–0.4 pH units was observed in the subsurface horizons (0–10 cm) compared with the pH of the seawater from the bottom horizons. The TA in the porewaters was significantly higher than that in the overlying seawater. The anaerobic degradation of organic matter is probably the main cause for the increasing TA in the sediments. The porewaters were significantly undersaturated with calcite and aragonite, except in that from the shallowest station, where the sediments below 7.5 cm were saturated, and even supersaturated, with calcite and aragonite. A linear correlation between the dissolved inorganic carbon and the TA for sediments with a slope of 0.9993 was found, despite there being potentially different ways for the diagenesis of the organic matter to occur. The diagenesis of organic matter in the top sediments of the JES forms gradients of TA and CO_2* concentrations on the interface of "bottom water–sediments". Averaged fluxes of TA and dissolved inorganic carbon (DIC) from the sediments to the bottom waters estimated by means of Fickian diffusion were calculated as 44 and 89 mmol/(m^2 year) for TA and DIC, respectively.

Keywords: carbonate system; marine sediments; acidification; Japan/East Sea

Citation: Tishchenko, P.; Zhang, J.; Pavlova, G.; Tishchenko, P.; Sagalaev, S.; Shvetsova, M. Revisiting the Carbonate Chemistry of the Sea of Japan (East Sea): From Water Column to Sediment. *J. Mar. Sci. Eng.* **2022**, *10*, 438. https://doi.org/10.3390/jmse10030438

Academic Editors: George Kontakiotis and Weidong Zhai

Received: 26 January 2022
Accepted: 10 March 2022
Published: 17 March 2022

1. Introduction

The carbonate system in seawater is one of the most important topics in modern oceanography. This system inherently links such global processes as acidification of the world's ocean [1–4] and eutrophication of the coastal ocean [5,6]. Both global processes occur in the Sea of Japan (East Sea) (JES) and can play an important role in the geochemistry of the carbonate system. Using experimental data of total alkalinity (TA), pH, and dissolved inorganic carbon (DIC) obtained in 1992, 1999, and 2007 for depths of 50–1000 m, Kim et al. [7] estimated the effect of anthropogenic CO_2 on the saturation depth for aragonite ($\Omega_a = 1$). The anthropogenic CO_2 that accumulated in the JES from 1800 to 1999 has variably displaced the $\Omega_a = 1$ depth upward by 50–250 m [7]. There is strong experimental evidence that acidification of the JES occurs due to the increasing carbon dioxide partial pressure in the atmosphere [8]. It was found that the acidification rate near the bottom of the JES is 27% higher than the rate at the surface [9]. Based on detailed hydrological and hydrochemical surveys conducted during the 2006–2012 period, seasonal hypoxia

caused by eutrophication was discovered in the Peter the Great Bay of the JES [10,11]. There is increasing atmospheric anthropogenic nitrogen precipitation on the surface of the JES [12], which may be one of the reasons for the acidification of the interior JES [13,14]. The carbonate chemistry of the JES has been extensively studied [15–20], particularly in recent years [21–23].

However, our knowledge regarding the carbonate system parameters in the sediments of the JES is much more limited. In specific areas of the JES, active geochemical processes impact the carbonate system parameters of the bottom waters [24]. The most important are the results obtained under the umbrella of the Ocean Drilling Program [25,26] and during the study of the sulfate methane transition zone in the Ulleung Basin of the JES [27]. The state of the carbonate system of seawater, especially the saturation degree depth of calcium carbonate, impacts the sediment composition and calcium carbonate preservation in the ocean [28,29]. We believe that the main reason for the gaps in the study of the carbonate system in sediments is methodological problems with sediment and porewater sampling, and the measuring parameters for the carbonate system.

There are two main approaches for studying the carbonate chemistry of marine sediments. The first includes in situ measurements of the parameters and/or sampling [30–33], and the second includes the recovery of sediment cores with a consequential sampling of the porewaters and measurement of the carbonate system parameters on board ships [34–36]. Both approaches have limitations. The second approach was used in this study. During the R/V *Hakuho Maru* KH-10-2 cruise, sediment samples were recovered from five stations using a multiple corer. The pH values of the sediments and the TA of the porewaters were measured on board the R/V. For the same stations, carbonate system parameters were measured in water columns. The profiles of the measured TA, calculated $pH_{\text{in situ}}$, and saturation degrees of calcite from the water columns and sediment cores are compared and discussed. The carbonate system of sediments of the JES is presented for the first time.

2. Study Area

The JES is very well ventilated at all depths from the surface to the bottom, and oxygen in the intermediate waters is higher than in adjacent basins [37]. The subpolar front separates the JES into northern and southern parts at approximately 38° N–40° N. For this reason, stations located near the KH-10-2 cruise crossed a subpolar front (Figure 1).

The chemical composition of the sediments reflects and is controlled by the type of sedimentary environment, which mostly contains the productive processes of the studied area. There is almost no phytoplankton with carbonate skeletons in the JES [38]. Copepods form a major part of the zooplankton [39]. In the southern part of the JES on the shelf, foraminifera plays an important role in forming carbonaceous sediments [40]. A general view of the sediments of the JES is presented in [41]. According to that study, the sediments on the shelves and bank tops are largely coarse-grained green and moderately calcareous sands containing less than 1% organic carbon. Those on the basin slopes are fine-grained green (grading to olive-brown below a depth of approximately 1800 m) and slightly calcareous silts containing 1–2% organic carbon. Yellow-brown clayey silts containing less than 1% $CaCO_3$ and less than 1% organic carbon were found below a water depth of approximately 2000 m covering the seafloor of the JES. These deepest sediments approach the character of red clay that occurs in the open ocean primarily at depths of more than 3000 m.

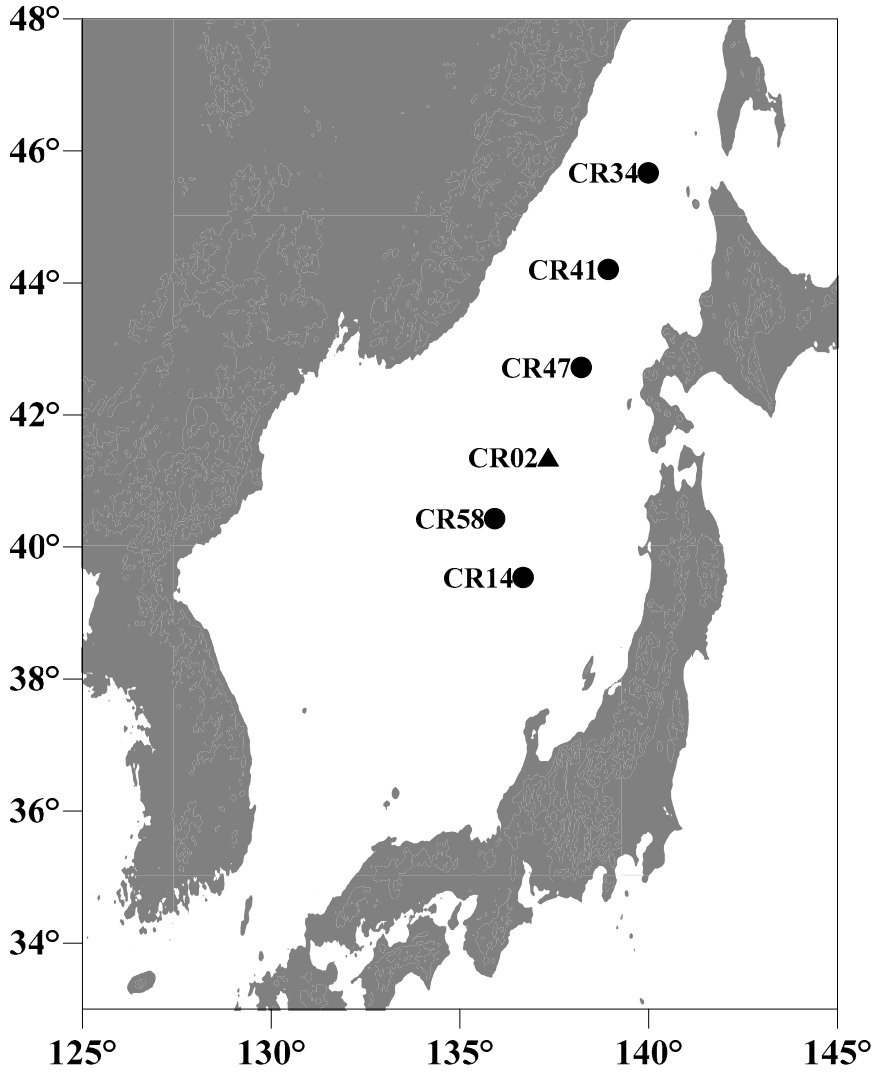

Figure 1. Locations of the hydrochemical and geochemical stations in the Japan/East Sea KH-10-02, 2010.

3. Methods

Location and sampling. During the R/V *Hakuho Maru* KH-10-2 cruise of five stations in the JES, samples of seawater and top sediments were collected for TA and pH measurements. The station locations are shown in Figure 1. A CTD-Carousel multi-sampling system (Seabird, SBE-32) was used to sample the seawater via 12 L Niskin bottles and to provide CTD (Seabird, Model SBE-911-plus) profiles. Seawater samples were drawn as soon as possible after the rosette with the Niskin bottles was brought onto the deck. Plastic flasks with a screw cap and approximately a 1 L volume were used for the pH/TA sampling. The sediment samples were recovered using a multiple corer fitted with eight 60 cm polycarbonate core tubes with a 9 cm diameter. The core samples were kept in a cold room (approximately 4 °C) immediately after recovery. The overlying supernatant water was placed into a 1 L plastic bottle using a siphon system for further determination of the pH and TA. This supernatant water was accepted as "zero" horizon in the sediment core. The pH values were measured for each sediment layer that was 3 cm thick. After the pH measurements, each layer was sliced and put into a squeezer. Porewater samples were obtained by squeezing the given sediment layer, and the TA was then measured for these samples.

Calcium measurements in porewater. The samples for the determination of dissolved calcium in porewater were acidified by supra HCl acid and were stored in the refrigerator

at 4 °C before analysis at the shore-based laboratory in POI (Pacific Oceanological Institute). Dissolved calcium in porewater was analyzed by complexometric titration of 1 mL of porewater dispensed in 10 mL of deionized water using the same procedure as with seawater analyses [42]. A Brinkman/Dosimat 665 motor-driven piston burette reproducible to ±0.001 mL in the delivered volume was applied for analysis. Based on the analysis of porewater replicates, an analytical precision of ±10 µmol/kg (n = 8) for calcium in porewater was achieved in this study.

Ammonium measurements in porewater. Ammonium was analyzed applying standard photometric procedures on a UV/VIS spectrometer model mini 1240 (Shimadzu) [43]. For the ammonia determination, 1 mL water samples or standards were diluted with 4 mL Milli-Q water, and 0.2 mL phenol solution was added. After 2 min, 0.1 mL citrate buffer and 0.2 mL DTT reagent were added, and the samples were kept at room temperature protected from sunlight for approximately 24 h before the absorbance of indophenol was measured at 630 nm. The precision of this method is ±0.01 µmol/L.

TA measurements. Bruevich's method was used for the determination of the TA in seawater and porewater [44]. This method can provide measurements for small volumes of samples (1 mL) [45], which is important for studying porewater samples. This method involves direct colorimetric titration by hydrochloric acid in an open cell using a mixed indicator (methylene blue and methyl red). The titration was performed under CO_2-free conditions by flushing the sample with argon during titration. The equivalence point was visually detected. The acid was calibrated by Dickson's CRM [46], which was performed at each station. The analytical precision was ±2.5 µmol/kg.

The CRM and seawater samples were titrated using a Dosimat 665 motor-driven piston burette (10 mL, with reading resolution ±0.001 mL). The solution color at the endpoint of the titration must change from green to light pink and be stable (no change for 1 min). The total titration time requires approximately 7 min. The intercalibration method for measuring the TA in seawater was demonstrated to be in good agreement, within ±1 µmol/kg [44] for Bruevich's method, with the Dickson method, which was certified by the National Bureau of Standards, USA [42]. Our TA data were systematically higher on 4 µmol/kg with SD = 2 µmol/kg compared with the ones obtained in 1999 [17] for the nearest stations (60, 64, 95, 109, 112, 135). Assuming that TA has no temporal dependence, 4 µmol/kg was subtracted from the original TA values obtained in this cruise.

Samples of the porewater were analyzed for TA 2–3 hours after squeezing. In this case, 1 mL of porewater dispensed in 10 mL of deionized water was titrated using the same procedure as described above for the seawater. Bruevich's method is convenient for working with small volumes of samples, avoiding the errors caused by H_2S oxidation during titration by flushing the titrated solution with argon [44]. Replicate measurements (n = 8) indicated stable values, and an analytical precision of ±10 µmol/kg for the total alkalinity in the porewater was achieved in this study.

pH measurements were performed using a cell without a liquid junction:

$$\text{glass} - \text{electrode} - \text{Na}^+ \left| \begin{array}{c} \text{test} - \text{solution} \\ (\text{reference} - \text{solution}) \end{array} \right| \text{H}^+ - \text{glass} - \text{electrode} \quad (\text{A})$$

The theoretical background of the application of the above cell for pH measurements in seawater has been provided elsewhere [47,48]. EMF (electromotive force) measurements of the cell (A) allow for the calculation of the pH using the following equation:

$$\begin{aligned} \text{pH}_\text{T} = {} & p(a^\text{P}_\text{H}/\gamma^\text{P}_\text{Na})_\text{s} + \tfrac{F(E_\text{s}-E_\text{x})}{RT\ln(10)} + \log\left[\tfrac{(m_\text{Na})_\text{s}}{(m_\text{Na})_\text{x}}\right] - \log\left[(\gamma^\text{P}_\text{Na})_\text{x}\right] + \\ & \log\left[(\gamma^{p}_{H})_\text{x}\right] - \log\left(1 - 0.00100511 \cdot \text{S}\right) \end{aligned} \quad (1)$$

where R, T, and F are the gas constant, Kelvin temperature, and Faraday number, respectively; $p(a^{P}_{H}/\gamma^{P}_{Na})_{s} \equiv -\log(a^{P}_{H}/\gamma^{P}_{Na})_{s}$ illustrates the assigned value of the standard buffer solution used for the calibration of cell (A); E_s and E_x represent the EMF of cell (A) measured in the standard and test solution, respectively; $(m_{Na})_s$ and $(m_{Na})_x$ denote the molalities of sodium ions in the standard and test solution respectively; $(\gamma^{P}_{Na})_x$ and $(\gamma^{P}_{H})_x$ constitute the activity coefficients of sodium and hydrogen ions, respectively, in the test solution on the "Pitzer scale" [48–50]; S is the salinity; and pH_T represents the pH of the test solution on the "total concentration of hydrogen ion scale", which is generally accepted [51]. Using the model of the chemical composition of major ions in seawater suggested by [52], the relationship between the molality of Na^+ and salinity can be obtained as follows:

$$(m_{Na})_x = 13.387 \cdot S/(1000 - 1.00511 \cdot S) \quad (2)$$

The calculations that take into account the activity coefficients of sodium, $(\gamma^{P}_{Na})_x$, and hydrogen, $(\gamma^{P}_{H})_x$, ions in seawater are described in detail in [48].

The pH of the seawater was measured as soon as possible after sampling using a pH meter, which contained two high-impedance inputs (Orion, model EA 940). The two glass electrodes (sodium and pH) were connected to a pH meter via high-impedance inputs, and one reference electrode was connected to both "ref" inputs on the pH meter. The EMF values from two channels of the pH meter were read out when the temperature of the sample reached 15 °C. The difference between the two EMF values of these channels provided the value of the EMF of the cell (A). The main body of the JES has a low temperature; to prevent bubble formation inside the cell, we measured the pH at 15 °C, rather than at the commonly accepted temperature of 25 °C.

Cell (A) was calibrated using a TRIS-TRISHCl-NaCl-H_2O buffer solution as the primary standard. The composition of the buffer solution was: $m_{NaCl} = 0.4$; $m_{TRIS} = m_{TRISHCl} = 0.04$. The values of $p(a^{P}_{H}/\gamma^{P}_{H})_s$ as a function of the ionic strength and temperature are given in [42]. At t = 15 °C and I = 0.44, the $p(a^{P}_{H}/\gamma^{P}_{H})_S = 8.3986$. The buffer solution was poisoned by a saturated solution of mercury chloride added at 200 µL per 1 L. The rubber stopper on the bottle with the buffer solution included an ascarite tube to prevent the buffer from being contaminated by CO_2 in the air. The buffer solution was transferred into the cell using a siphon system. After half an hour, the EMF values for cell (A) were read out over 10 min. The pH of the seawater on the "total concentration of hydrogen ion scale" was calculated via the equation:

$$\begin{aligned}(pH_T)_{t=15} = 8.3986 + \tfrac{F(E_s - E_x)}{57.167} + \log(0.4) - \log[13.387 \cdot S/(1000 - 1.00511 \cdot S)] - \\ \log[(\gamma^{P}_{Na})_x] + \log[(\gamma^{p}_{H})_x] - \log(1 - 0.00100511 \cdot S)\end{aligned} \quad (3)$$

From the measured EMF data of cell (A) and from the salinity data, the pH vales of the seawater samples at 15 °C were obtained using Equation (3). The typical reproducibility of cell (A) was approximately ±0.2 mV, which is equivalent to ±0.004 pH units.

The pH of the sediments was measured with almost the same equipment as that used for the pH measurements of the discrete seawater samples, except for the pH meter. A pH meter from Orion (model 720) was used to measure the pH of the sediments. To minimize the degassing process for the sediments, the measurements were performed in a cool room with an ambient temperature of approximately 3–5 °C. Before the measurements, the electrodes for cell (A) with a temperature probe were rinsed using seawater from the bottom horizon and wiped with a Kimwipe. They were then punched into the sediment at a 2–3 cm depth, and the EMF of cell (A) was recorded by computer over 20–25 min. The typical time dependence of the EMF in the sediments is shown in Figure 2.

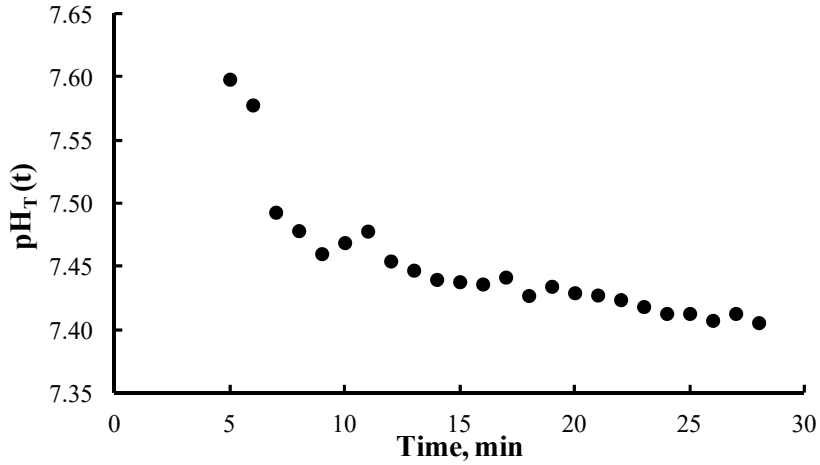

Figure 2. Time dependence of the measured pH_T in the sediment core (Station CR14).

Next, electrodes were removed from the sediments and put into a cap containing seawater from the bottom horizon. The core was pushed up from the bottom of the polycarbonate core tubes to 3 cm. The 3 cm-thick layer was sliced to obtain porewater, and the next layer was then ready for pH measurement. Cell (A) was calibrated using a TRIS-TRISHCl-NaCl-H_2O buffer solution at 3, 5, 7, and 10 °C, and the E_s values as a function of temperature were obtained (Figure 3).

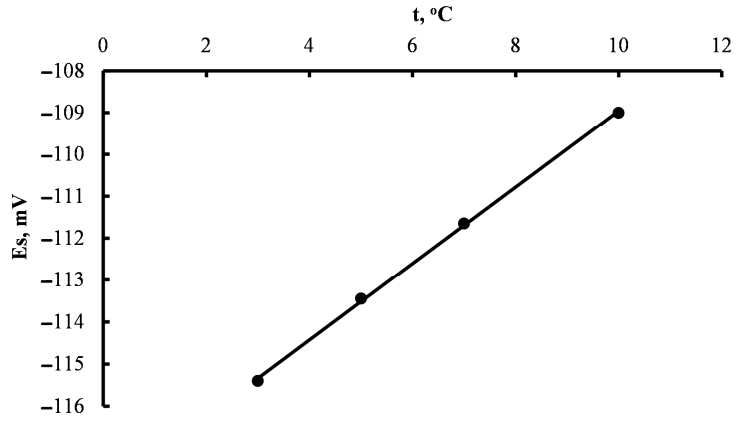

Figure 3. The temperature dependence of cell (A) in the TRIS-TRISHCl-NaCl-H_2O buffer solution ($m_{NaCl} = 0.4$; $m_{TRIS} = m_{TRISHCl} = 0.04$). Station CR14 (39°32.316′ N; 136°40.416′ E), KH-10-02, 17 June 2010, JES. $(E_s)_t/mV = -118.07 + 0.9112 \cdot t$; $r^2 = 0.9995$.

The pH values of the sediments for a given temperature, t, were calculated using the following equation:

$$[pH_T]_t = [p(a^P_H/\gamma^P_{Na})_s]_t + \frac{F(E_s - E_x)_t}{RT\ln(10)} + \log(0.4) - \log[13.378 \cdot S/(1000 - 1.00511 \cdot S)] - \log[(\gamma^P_{Na})_x]_t + \log[(\gamma^P_H)_x]_t - \log(1 - 0.00100511 \cdot S) \quad (4)$$

Here, "t" is the temperature at which the EMF of cell (A) was measured in the sediment core. The $(E_s)_t$ values were calculated using the empirical relationship:

$$(E_s)_t = a + b \cdot t \quad (5)$$

The empirical coefficients "*a*" and "*b*" were obtained by the least square method using calibration data (Figure 3). This method prevents any errors regarding the liquid junction potential, which can be unusually high in reduced sediments [34]. However, the used pro-

cedure has potential errors, such as the degassing and oxidation of the sediment during pH measurement. For this reason, the period of each measurement was no longer than 25 min, and at the end of this period, the scatter of recoded pH values did not exceed ±0.01 pH unit. The error of the pH measurements in the sediment was adopted as ±0.01 pH unit.

The seawater pH_T data obtained at 15 °C (Equation (3)) and the $(pH_T)_t$ of the sediments obtained at temperature "t" (Equation (4)) should be considered as the carbonate parameters that can be used with the TA to calculate all other parameters of the carbonate system.

Calculation of carbonate system parameters

Dickson [53] provided an exact definition of TA that included fluoride, sulfate, borate, silicate, ammonia, and hydrogen sulfide in basic form (acceptor H^+) and acid form (donor H^+) regarding zero level (pK = 4.5):

$$TA = [HCO_3^-] + 2[CO_3^{2-}] + [B(OH)_4^-] + [OH^-] + [HPO_4^{2-}] + 2[PO_4^{3-}] + [HS^-] + [SiO(OH)_3^-] + [NH_3] + \ldots - [H^+] - [HF] - [H_3PO_4] - [HSO_4^-] - [HNO_2] - \ldots \quad (6)$$

At natural pH waters (7–8), Equation (4) is significantly simplified:

$$TA = [HCO_3^-] + 2[CO_3^{2-}] + [B(OH)_4^-] + [HPO_4^{2-}] + 2[PO_4^{3-}] + [SiO(OH)_3^-] + [HCO_3^-] + [HS^-] + [NH_3] + [OH^-] \quad (7)$$

For an aerobic basin with a high nutrient concentration, Equation (7) is reduced as follows:

$$TA = [HCO_3^-] + 2[CO_3^{2-}] + [B(OH)_4^-] + [HPO_4^{2-}] + 2[PO_4^{3-}] + [SiO(OH)_3^-] + [HCO_3^-] + [NH_3] + [OH^-] \quad (8)$$

However, for an aerobic basin such as the JES with a low nutrient concentration, Equation (7) is reduced to sum carbonate and borate alkalinity [54]:

$$TA = DIC\frac{(K_{1C}a_H + 2K_{1C}K_{2C})}{(a_H^2 + a_HK_{1C} + K_{1C}K_{2C})} + B_TK_B/(a_H + K_B) + K_W/a_H \quad (9)$$

where: K_{1C} and K_{2C}, and K_B, are apparent dissociation constants of carbonic and boric acids, respectively; K_W represents ionic products of water; B_T stands for the total concentration of borax in seawater, which is calculated from the known salinity of the sample by the relationship: $B_T = 0.000416(S/35)$ [55]; a_H is hydrogen ion concentration ($a_H = 10^{-(pH_T)}$); and DIC is defined as follows:

$$DIC = [CO_2^*] + [HCO_3^-] + [CO_3^{2-}] \quad (10)$$

where $[CO_2*] = [CO_2]_{dissolved\ gas} + [H_2CO_3]_{molecular\ carbonic\ acid}$ [56]. We calculated the DIC by means of Equation (9) for seawater and porewater using the measured TA and pH_T data. In this case, the dissociation constants in the "total hydrogen concentration scale" were taken from [56]. TA and DIC are invariant with respect to temperature and pressure, and permit the calculation of $pH_{in\ situ}$ [54], using dissociation constants for the given temperature, salinity, and pressure. The pressure effect on the dissociation constants was taken into account according to recommendations by Millero [55], which provided relationships for calculations of solubility products of calcite (Ksp_c) and aragonite (Ksp_a). Thus, we were able to calculate the saturation degrees Ω_c and Ω_a of seawater and porewater with respect to calcite and aragonite, respectively:

$$\Omega_c = [Ca^{2+}] \cdot [CO_3^{2-}]/Ksp_c;\ \Omega_a = [Ca^{2+}] \cdot [CO_3^{2-}]/Ksp_a \quad (11)$$

where $[Ca^{2+}]$ and $[CO_3^{2-}]$ are concentrations (mol/kg) of calcium and carbonate ions, respectively. The calcium concentration for porewaters in the studied samples are given

in Table S1 in the Supplemental Materials. The calcium concentration for seawater was calculated by the relationship $[Ca] = 0.01028 \cdot S/35$ [55], which is in good agreement with the original calcium data for the JES [20]. The errors caused by neglecting other acid-base systems on the calculated carbonate system parameters will be discussed later.

All statistical tests were performed using statistics software for Excel. A regression analysis (i.e., LSM) was performed to obtain empirical relationships between the chemical variables. The statistical tests were characterized by the 95% confidence interval (i.e., $p < 0.05$) and R^2.

4. Results and Discussion

Water column. The concentrations of silicates and phosphates in the seawater of the JES are in ranges from 0.75 to 91 and 0.02 to 2.1 µmol/kg, respectively (Talley et al., 2004). Using nutrient, pH, and alkalinity data obtained in 1999, the contribution of silicates and phosphates on the calculated carbonate system parameters was taken into account. The effects vary from 0 to 3 µmol/kg in DIC, ±0.01 in saturation degree, and less than 0.001 pH unit. Thus, the errors caused by neglecting the contribution of silicates and phosphates on the calculated parameters of seawater are significantly less than the experimental ones.

The calculated $pH_{in\ situ}$ data are presented in Figure 4. The in situ pH values obtained in this cruise for horizons below 500 m are systematically lower compared to the ones obtained in 1999 [17] for the nearest stations (60, 64, 95, 109, 112, 135), as demonstrated in Figure 4.

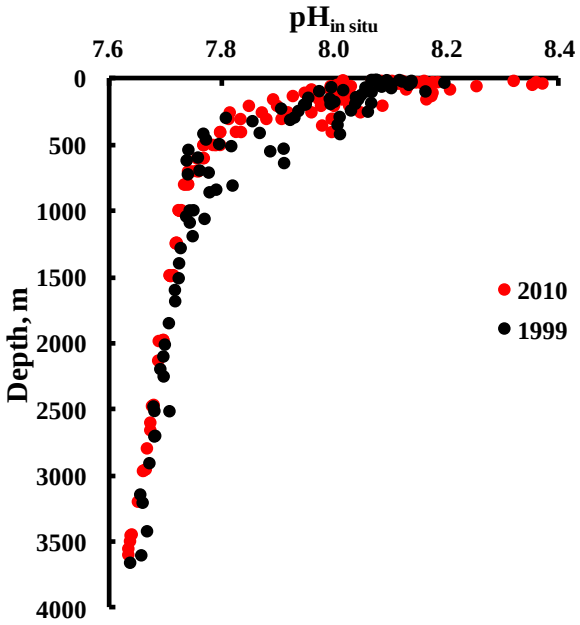

Figure 4. Vertical distribution of $pH_{in\ situ}$ (total of hydrogen concentration scale, [51]) in seawater of the JES. Red points represent data obtained in 2010 (R/V *Hakuho Maru* KH-10-2); black points represent data obtained in 1999 (R/V Revelle, Khromov).

The vertical distributions of the carbonate system parameters—normalized nTA (nTA = TA × 35/S), $pH_{in\ situ}$, and Ω_c, Ω_a (saturation degree indices of calcite and aragonite, respectively)—in the seawater column in the JES are presented in Figure 5. To exclude the effects of atmospheric precipitation/evaporation and ice formation/melting, nTA is used rather than TA [57]. Except for station CR14, the profiles of nTA demonstrate a distinct minimum corresponding to 200–250 m depths. The upper layer (10–75 m) of the CR14 station has a maximum salinity (34.081–34.140) indicating the Tsushima Warm Water masses [37], which have low nTA (Figure 5; [15]). For this reason, the nTA profile of the CR14 station does not reveal a minimum. The minimums revealed on nTA profiles were

observed before, and it was suggested that the minimum core of nTA originates from the Kuroshio region, which has low nTA [15]. It should be noted that photosynthesis and aerobic remineralization of organic matter impacts TA [57,58]. Using Redfield stoichiometry [59] for organic matter, the process of aerobic respiration can be formally represented by the following scheme:

$$(CH_2O)_{106}(NH_3)_{16}H_3PO_4 + 138 \cdot O_2 \rightarrow 106 \cdot CO_2 + 122 \cdot H_2O + 16 \cdot HNO_3 + H_3PO_4 \quad (12)$$

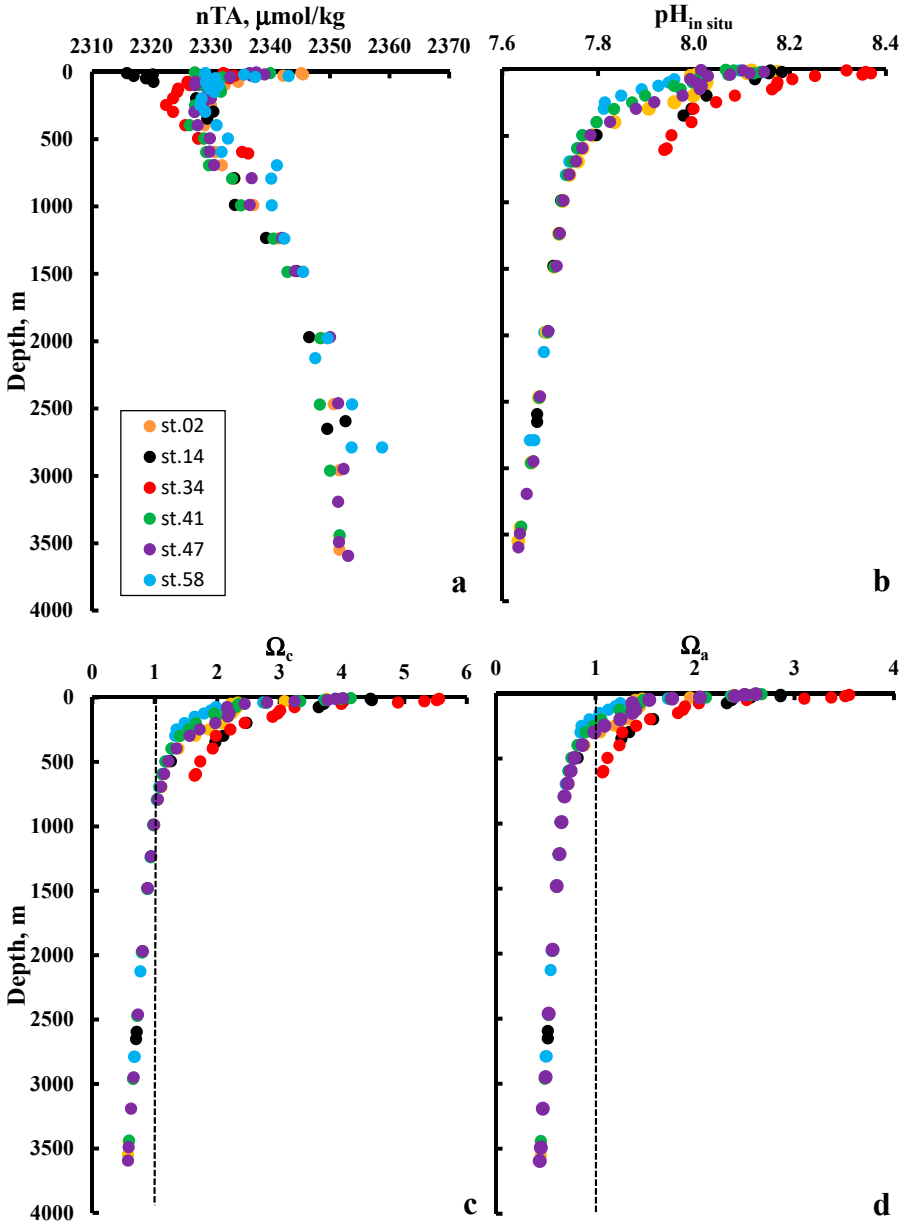

Figure 5. Vertical distributions of the carbonate system parameters for the seawater: (**a**)—normalized TA (nTA = TA × 35/S); (**b**)—$pH_{in\ situ}$; (**c**)—saturation degree indices of calcite; (**d**)—saturation degree indices of aragonite.

It should also be noted that aerobic remineralization of organic matter possibly also contributes to the formation of a minimum vertical distribution of nTA (Figure 5).

The saturation degree of calcite and aragonite continuously decreases with depth due to pressure and temperature effects on the solubility of solid calcium carbonate. The average depths of calcite and aragonite saturation for the five stations (CR41, CR47, CR02,

CR58, CR14) were 960 m and SD = 12 m, and 286 m and SD = 87 m, respectively. Our estimations of the saturation depth for calcite and aragonite involved potentiometric pH and Bruevich's data for the TA obtained in 1999 for five stations in a similar region (60, 64, 95, 109, 112, 135; [17]), which were 1132 m with an SD = 80 m, and 386 m with an SD = 133 m. In the early 1990s, however, saturation degrees were obtained at depths 1300 m and 300 m for calcite and aragonite, respectively [15]. There is great uncertainty in the estimation of aragonite saturation depth due to mostly intense mesoscale water dynamics above 500 m [60].

Nevertheless, the main difference between the calcium carbonate (calcite and aragonite) saturation depths in 1999 and 2010 is likely to be the interior acidification of the JES [7,9,13,14]. Systematically, the differences in $pH_{\text{in situ}}$ values between the two datasets (1999 and 2010) demonstrated in Figure 2 are additional evidence supporting the notion that acidification of the interior of the JES occurs. For a qualitative estimation of the acidification, all the pH data were grouped into five depth intervals: 500–1000 m, 1000–1500 m, 1500–2000 m, 2000–2500 m, and 2500–3400 m. Each group contained, as a minimum, 10 original pH values. Within each group, for a given year (1999 and 2010), the pH values were calculated for nominal depths (750, 1250, 1750, 2250, and 3000 m) using the empirical dependences of given parameters as functions of depth. These empirical dependences were obtained using the least squares method (LSM). Each value, corrected for nominal depth (i), was then used for the estimation of a temporal variability rate as follows:

$$R^{i}_{pH} = [pH^{i}_{2010} - pH^{i}_{1999}]/(2010 - 1999) \quad (13)$$

where superscript "i" is nominal depth. In Table 1, the averaged acidification rates and SD are compared with those obtained for the north-western part of the JES [13].

Table 1. Acidification rates (pH unit/year) of the JES at different depths in the north-western [36] and eastern parts (this study).

Depth	Rate [(1)]	SD [(1)]	Rate [(2)]	SD [(2)]
750	−0.0030	0.00035	−0.0038	0.0010
1250	−0.0018	0.00019	−0.0017	0.0005
1750	−0.0009	0.00012	−0.0010	0.0004
2250	−0.0006	0.00015	−0.0006	0.0002
3000	−0.0007	0.00016	−0.0011	0.0003

[(1)] Acidification rates in the eastern part of the JES and its standard deviations are estimated in this study, using $pH_{\text{in situ}}$ data obtained in 1999 and 2000 years (Equation (13)); [(2)] Acidification rates in the north-western part of the JES and its standard deviations are estimated in [13].

Despite the large SD in estimations of the acidification rates in this paper (Table 1), they are in good agreement with those obtained before for the north-western part of the JES. In other words, the acidification rate is very similar for the whole JES. It has been documented that a decrease in dissolved oxygen [9,61] and an increase in nutrients and DIC [13] has occurred in the JES. This suggests that the remineralization of organic matter (Equation (9)) in the interior of the JES is not a steady-state process.

Our results demonstrate that the measured pH and DO (dissolved oxygen) concentrations in intermediate, deep, and bottom water masses have been decreasing over recent years [36]. On the other hand, calculated NDIC (normalized dissolved inorganic carbon), pCO_2–CO_2 partial pressure, and measured nutrient concentrations have been increasing. Maximum rates of acidification and deoxygenation are occurring at around 750 m. The annual rate of pCO_2 increase in the water exceeds the atmospheric rate more than two times at a depth of 750 m. The observed variability in the hydrochemical properties can be explained by the eutrophication of the JES, rather than by the cessation of the ventilation of the deep waters [36]. A modeling study of the acidification of the deep and bottom waters

of the JES suggests that a combination of reduced deep/bottom water formation and an increase in organic matter remineralization can best explain the observed pattern of rapid acidification in deep waters [14].

The interior acidification of the JES impacts such geochemical parameters as "lysocline" depth and "compensation depth". According to [29], mid-depth sediments are rich in $CaCO_3$, and those from abyssal depths are devoid of $CaCO_3$. These two realms are separated by a transition zone that spans several hundreds of meters in water depth, over which the $CaCO_3$ content drops toward zero from the 85–95% values that characterize mid-depth sediment. The upper bound of this transition zone has been termed the "lysocline" and signifies the depth at which dissolution impacts become noticeable. The lower bound is termed the "compensation depth" and signifies the depth at which the $CaCO_3$ content is reduced to 10% [62]. Adopting a saturation degree of 91% as a qualitative reference for the lysocline depth of calcite [63], the average depths for the five stations were 1500 m with an SD = 21 m, and 1360 m with an SD = 12 m in 1999 and 2010, respectively. Using a saturation degree of 80% as the reference calcite compensation depth or CCD [63], the average depths for the five stations were 2100 m with an SD = 70 m, and 1980 m with an SD = 14 m in 1999 and 2010, respectively. Despite the large uncertainty in the estimation of the lysocline and CCD depths, the main differences in the values for 1999 and 2010 can be attributed to the acidification of the JES. Ichikura and Ujiie [64] reported that diatomaceous yellowish-brown or brown clays are widely distributed over the deep seafloors of the Japan, Yamato, and Ulleung basins. They estimated a CCD between 1500 and 2000 m due to the occurrence of planktonic foraminifera [64].

Sediments. The application of Equation (9) is too simplified to study the carbonate system of the sediments as, due to the early diagenesis of organic matter, nutrient concentrations may be significantly increased in the porewater. Indeed, our analysis of the JES seawater demonstrated trace concentrations of ammonium (as a rule, less than 1 μmol/L) during the expedition on R/V Khromov 2000. Ammonium concentrations of porewaters reach 40 μmol/L (Table S1). Unfortunately, we were not able to carry out an analysis of phosphorus and silica concentrations in porewaters during the cruise. However, these concentrations may be estimated using two assumptions. First, the hydrochemical properties of the deep waters of the JES are very uniform [17]. Therefore, the phosphorus and silica concentrations in the bottom waters can be accepted as 2 and 90 μmol/L, respectively, for all stations, except station 34, the depth of which is 554 m. Using published data [17], $[P]_b$ and $[Si]_b$ (subscript "b" meaning "bottom water") were estimated as 1.7 and 50 μmol/L, respectively. The second assumption is the application of the following ratios: N:P = 16 [56] and Si:N = 1.2 [65]. Thus, the estimated concentrations via the ammonium concentrations of the porewater samples (Table S1) for i horizons were $[P]_I = [P]_b + [NH_4]_i/16$ and $[Si]_I = [Si]_b + 1.2[NH_4]_I$, and are listed in Table S2. In this case, TA is defined by Equation (8). In the calculations of the carbonate system parameters of the sediments, the salinity and temperature of the bottom waters were also used for the dissociation constants and total borax concentration calculations.

The results obtained by means of Equations (8) and (9) were very similar. The differences in DIC values obtained by the two approaches did not exceed 5 μmol/kg. The differences in pH did not exceed 0.001 pH unit, and there was no change in the calculation of saturation degrees regarding calcium carbonates. We did not include the hydrogen sulfide acid-base system in our consideration, as sulfide ion is a very reactive species with regard to trace metals, and all forms of this system are intensively oxidized by any electron acceptors, and the sediments had no odor of H_2S. Below, the results obtained with the additional involvement of phosphate, silicate, and ammonium acid–based systems (Equation (9)) will be considered.

The parameters of the carbonate system, $pH_{in\ situ}$, TA, Ω_c, and Ω_a, are presented in Figure 6 for the sediments on the studied stations (Figure 1). These results support the generally accepted view that the pH of sediments gradually decreases compared with the above seawater, except for horizons below 7.5 cmbsf at the CR34 station. The porewaters

of all other studied sediments are undersaturated with calcite as well as aragonite. The supernatant waters have almost the same values of $pH_{in\ situ}$ and TA as those in the bottom waters for all stations, except for the CR34 station again, where the pH was lower compared with the values for the bottom water. Figure 6 demonstrates the sharp lowering of the pH by 0.3–0.4 pH units in the subsurface horizons (0–10 cm), which is caused by active biogeochemical processes within this top sediment layer. The TA in the porewaters is significantly higher than that in the overlying seawater. The anaerobic degradation of organic matter is likely the main cause for the increasing TA in the sediments. Of note, the most considerable increase in TA in the porewater was observed at the CR47 station, which is located in the subpolar front (Figure 1). A plot of the calculated DIC vs. TA in the sediments shows a linear correlation (Figure 7) with the following empirical relationship:

$$\mathrm{DIC}\ (\mu\mathrm{mol}\cdot\mathrm{kg}^{-1}) = 56.2 + 0.9993\cdot\mathrm{TA};\ r^2 = 0.98 \quad (14)$$

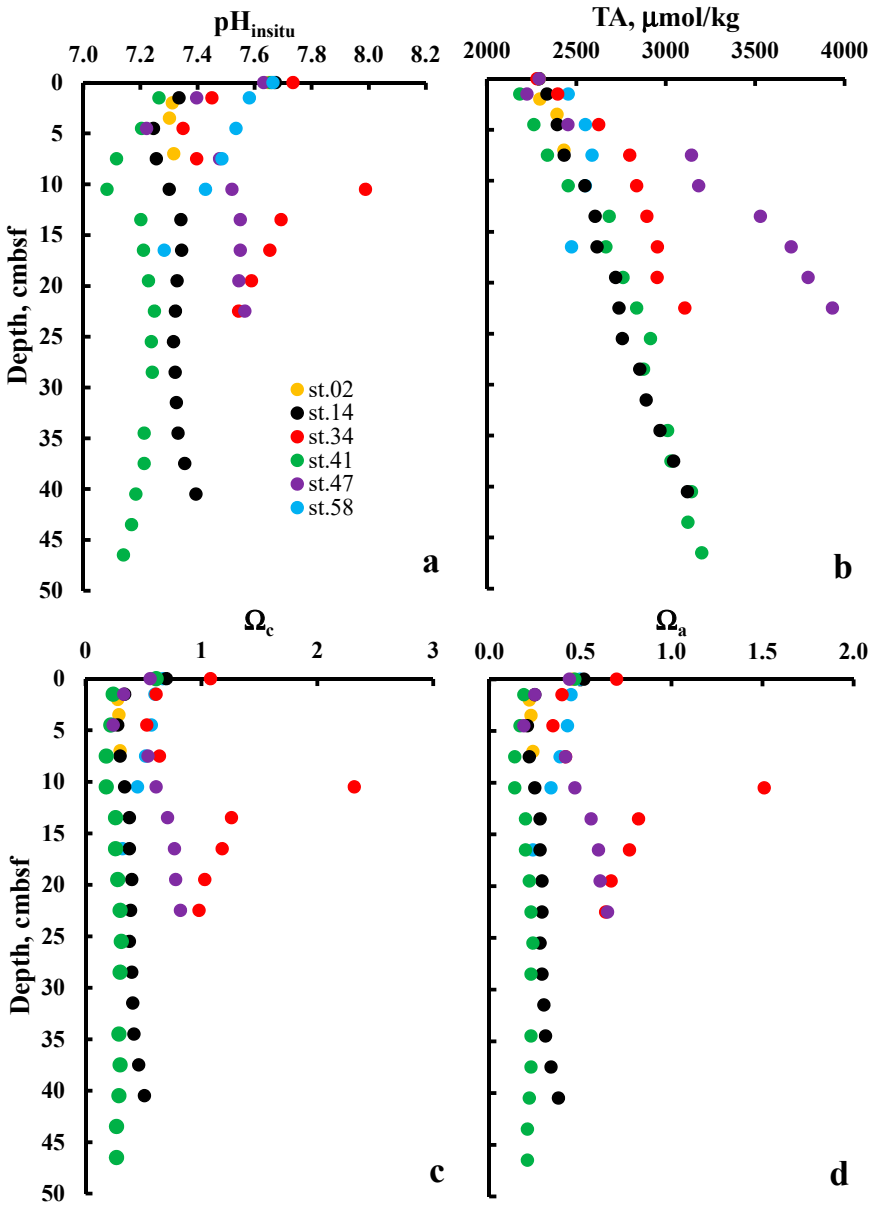

Figure 6. Vertical distributions of the carbonate system parameters for sediments: (**a**)—$pH_{in\ situ}$ (total hydrogen concentration scale, [51]); (**b**)—total alkalinity; (**c**)—saturation degree indices of calcite; (**d**)—saturation degree indices of aragonite.

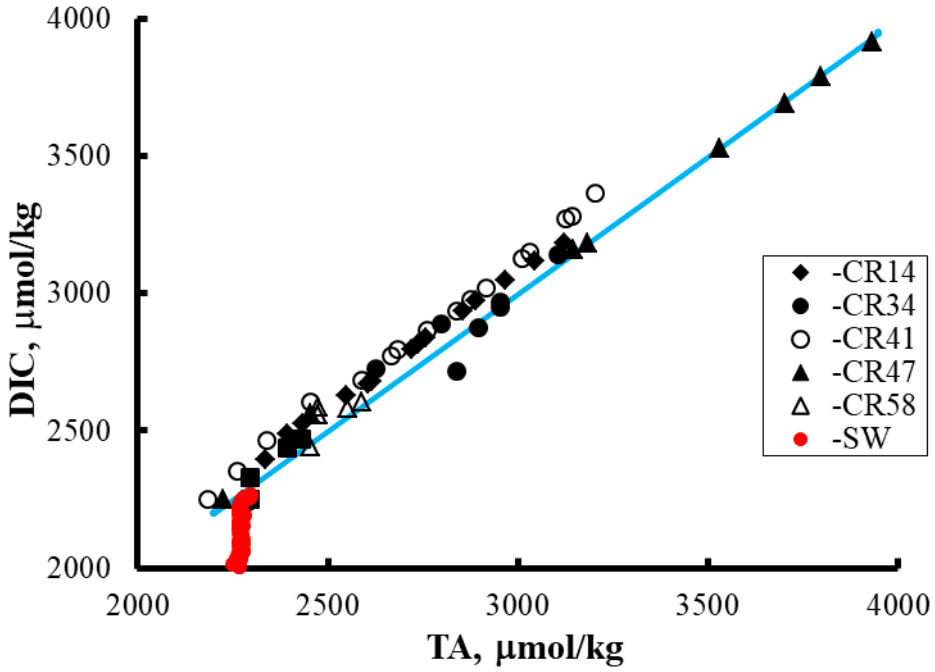

Figure 7. Relationship between DIC and TA in the sediments. The solid blue line was obtained using the least squares method. DIC (µmol/kg) = 56.2 + 0.9993 × TA; r^2 = 0.98, which closely corresponds to the theoretical relationship for the bacterial sulfate reduction that uses carbohydrates as the organic matter [33] when ΔDIC:ΔTA = 1. SW—measured TA and calculated DIC for the seawater column from all studied stations.

In contrast, DIC vs. TA in the seawater column of all stations shows an almost vertical line (Figure 7). This is unsurprising for seawater because the aerobic degradation of organic matter impacts slightly on the TA and significantly increases the DIC. The linear correlation of DIC from TA in the sediment can be explained by bacterial sulfate reduction [66]:

$$(CH_2O)_{106}(NH_3)_{16}H_3PO_4 + 53SO_4^{2-} \rightarrow 106HCO_3^- + 53H_2S + 16NH_3 + H_3PO_4 \quad (15)$$

According to Equation (15), the slope should be "1". However, Equation (15) is not the only reaction under anaerobic conditions; oxygen limitation initiates alternative electron acceptors by anaerobic organisms (mainly microbes). Following oxygen depletion, anaerobic respiration is sequentially based on nitrate, manganese, and iron hydroxides and sulfates [67,68]. The participation of different electron acceptors in the diagenesis of organic matter provides different relationships between TA and DIC. In this case [66]:

$$(CH_2O)_{106}(NH_3)_{16}H_3PO_4 + 94.4HNO_3 \rightarrow 106CO_2 + 55.2N_2 + 177.2H_2O + H_3PO_4 \quad (16)$$

$$(CH_2O)_{106}(NH_3)_{16}H_3PO_4 + 236MnO_2 + 472H^+ \rightarrow 106CO_2 + 366H_2O + 236Mn^{2+} + 8N_2 + H_3PO_4 \quad (17)$$

$$(CH_2O)_{106}(NH_3)_{16}H_3PO_4 + 424FeOOH + 848H^+ \rightarrow 106CO_2 + 742H_2O + 424Fe^{2+} + 16NH_3 + H_3PO_4 \quad (18)$$

Different electron acceptors provide different increases in DIC and TA. For Equations (16)–(18), the ratios of ΔDIC : ΔTA will be 106:94.4 (1.123), 106:471 (0.225), and 106:847 (0.125), respectively. In this case, we expect significant variations in the slope, depending on the DIC vs. TA. However, the solid calcium carbonate in sediments can

take part in the anaerobic oxidation process of organic matter and smooth the variations in the increases in DIC and TA [66]. Assuming that calcite provides saturation conditions in porewaters during the oxidation reaction, Equations (16)–(18) should be rewritten as follows [66]:

$$(CH_2O)_{106}(NH_3)_{16}H_3PO_4 + 94.4NO_3^- + 11.6[CaCO_3]_{solid} \rightarrow 117.6HCO_3^- + 55.2N_2 + 71.2H_2O + H_3PO_4 + 11.6Ca^{2+} \quad (19)$$

$$(CH_2O)_{106}(NH_3)_{16}H_3PO_4 + 236MnO_2 + 366Ca^{2+} + 260HCO_3^- \rightarrow 366[CaCO_3]_{solid} + 260H_2O + 236Mn^{2+} + 8N_2 + H_3PO_4 \quad (20)$$

$$(CH_2O)_{106}(NH_3)_{16}H_3PO_4 + 424FeOOH + 758Ca^{2+} + 652HCO_3^- \rightarrow 758[CaCO_3]_{solid} + 16NH_4^+ + 636H_2O + 2424Mn^{2+} + H_3PO_4 \quad (21)$$

Thus, solid-phase calcite precipitates during the oxidation of organic matter by hydroxides of manganese and iron (Equations (20) and (21)), or dissolves when organic matter is oxidized by nitrate (Equation (19)). In these cases, $\Delta TA = \Delta DIC$ and the relationship of DIC vs. TA will look like the result of Equation (15). The slope, b, in the relationship $DIC = a + b \cdot TA$ is almost "1" (Equation (14)) when all data are used. However, the slopes are widely ranged between the stations (Table 2), despite the parameter of a_o ($a_o = DIC_o - TA_o$); where DIC_o and TA_o are DIC and TA in supernatant waters) being almost the same for each station (Table 2). It should be noted that we did not use the actual measured Ca concentrations (Table S1) for the explanation slope in Figure 7, as we felt that the errors in the determined calcium concentrations were approximately 1%, despite the excellent method from Tsunogai [42]. Additional errors possibly arose due to the transportation of samples from R/V Hakuho Maru to POI (Vladivostok).

Table 2. Empirical parameters of linear dependences DIC vs. TA: a—intercept; b—slope; n—number measurements; R^2—the coefficient of determination and parameter of interstitial waters; and a_o ($a_o = DIC_o - TA_o$); where DIC_o and TA_o are DIC and TA in supernatant waters.

St	a	b	n	R^2	a_o
CR02	−860.3	1.373	4	0.89	−44
CR14	−47.4	1.044	15	0.99	−40
CR34	68.8	0.980	9	0.94	−32
CR41	−110.2	1.079	17	0.99	−45
CR47	84.0	0.978	9	0.997	−40
CR58	−536.1	1.230	6	0.85	−40

Evidently, if the diagenetic process in sediments is governed by Equation (15), the slope should be "1" with an intercept at approximately "−40". An increase in slope ($b > 1$; $a < -40$) can be provided by contributions from the following reactions: (1) the oxidation of H_2S by oxygen penetrated into the sediments; (2) Equation (16) without involving solid calcium carbonate; and (3) the interaction of H_2S with Fe^{2+}. The opposite situation can occur ($b < 1$; $a > -40$) when Equations (17) and (18) participate in the oxidation of organic matter rather than Equations (20) and (21). We have no additional geochemical information to make a preferable conclusion regarding the abovementioned reactions. The degassing of the sediment retrieved on board the ship will also result in $b < 1$ and $a > -40$. We suggest that this situation occurred at the CR34 station.

The bottom waters at the CR34 station at a depth of 554 m are supersaturated with calcium carbonate. However, the porewater is undersaturated with $CaCO_3$ in the top sediments within 0–7 cm due to anaerobic oxidation via bacteria and infauna. The observed supersaturation of porewater by calcite and aragonite at the 10.5 cm horizon is likely an

artifact that may be caused by the degassing of methane from the sediments. This station is not far from stations where near-bottom hydrochemical anomalies were observed, which are probably caused by the venting of methane from the sediments [24]. We suggest that the precipitation/dissolution of $CaCO_3$ provides the pH stabilization in the sediments that occurred above the CCD horizon (Equations (19)–(21)), in the case of the CR34 station. However, in the cases where sediments occurred below the CCD horizon (all stations except CR34), the calculations for the saturation degree obtained from the measured pH and TA demonstrate that porewaters are strongly undersaturated with calcium carbonate (Figure 6). The pH becomes quite stable 10 cm below the retrieved cores. In the sediments of these stations, the solid phase of calcium carbonate is not likely to be involved in the process of anaerobic degradation of organic matter. Nevertheless, there is a mechanism that provides a stable pH state in the sediments and a linear correlation between the TA and the DIC (Figure 7). Boudreau and Canfield [69] assumed that precipitation of FeS plays an important role in offering a pH-state mechanism in porewaters.

The effects of acidification on marine sediments have been widely discussed [70,71]. However, early diagenesis of organic matter in the sediments forms gradients of TA and DIC, on the interface of "bottom water–sediments". These gradients will generate fluxes, J_i, of carbonate system components from sediments into bottom water. Thus it may acidify bottom water. For estimation of this, we need knowledge about the fluxes of two parameters of the carbonate system. DIC, in this case, is not an appropriate parameter, because it is defined as the sum of three components (Equation (7)). Using pH and TA data, we calculated CO_2*. Profiles TA, DIC, and CO_2* are presented in Figure 8 for the CR41 station. Accepting $C_{HCO_3^-}$ = TA, fluxes of TA and CO_2* were estimated by means of Fickian diffusion [72]:

$$J_{\mathrm{i}} = -\varphi \cdot \frac{D_i^{sw}}{\theta^2} \cdot \left.\frac{\partial(C_i)}{\partial x}\right|_{\mathrm{x}=0} \quad (22)$$

where D_i^{sw}, $\partial C_i/\partial x$, φ, and θ represent the diffusion coefficient of specie "i" in seawater, the vertical gradient concentration of specie "i", porosity, and tortuosity, respectively. Using TA and CO_2* concentrations for five first horizons, their gradients on the interface of the "bottom water–sediments" were calculated. Adopting $\varphi = 0.8$ and $\theta^2 = 1.45$ for surface sediments [73], fluxes of TA and CO_2* from the sediments to the bottom water were estimated using Equation (22) and the available diffusion coefficient of HCO_3^- and CO_2* [73]. The estimated annual fluxes of TA and CO_2 were from 16 (CR14) to 99 (CR47) mmol/(m^2 year) and from 10 (CR58) to 69 (CR14) mmol/(m^2 year), respectively. The average fluxes were close: 44 and 45 mmol/(m^2 year) for TA and CO_2, respectively, and 44 and 89 mmol/(m^2 year) for TA and DIC. This result contradicts our finding presented in Figure 7. Indeed, Figure 8 demonstrates that TA concentration is a little lesser at 3 cm horizon than one for supernatant water and then it is monotonically increasing. However, increasing CO_2* concentration starts from supernatant waters. Such different behavior is probably caused by oxygen oxidation of H_2S. This process will result in a decreasing TA concentration and an increasing the CO_2* concentration and no change in DIC as we can observe in Figure 8. Obviously, this process will give slight random points of dependence of the TA vs. DIC, because the span of TA and DIC variations is large in comparison with the first 3–4 points regarding seawater/sediment interface. However, we have too little information for a discussion on this matter, a more detailed study is needed. Nevertheless, we do not exclude the acidification of seawater by sediments. This process is well known on the shelf [6]. If additional TA and CO_2* concentrations come up from the sediments into the bottom waters and mix within 10 meters, the increments in the TA and DIC will be 4.4 and 8.9 µmol/kg each year, respectively. Such an increment will give a drop pH of 0.016 pH unit within 10 meters of the bottom waters. That signal is measurable and can be detected. However, our study of the JES on R/V Hakuho Maru KH-10-2 cruise did not demonstrate such a decrease in pH. Data in 1999 on R/V Revelle demonstrated a decreasing pH of 0.02 pH unit (Figure 4). Furthermore, extensive study on the JES in 1999 [17] permitted that an established hydrochemical anomaly caused geochemical activity

on the continental slope in the region of the Tatar Strait and in the southwestern slope of the Tsushima Basin [24]. The occurrence of intensive mixing of waters is possibly the main reason TA and DIC fluxes were not experimentally detected from sediments in the bottom waters. Additional study of the interaction of the seawater/sediment interface is clearly needed.

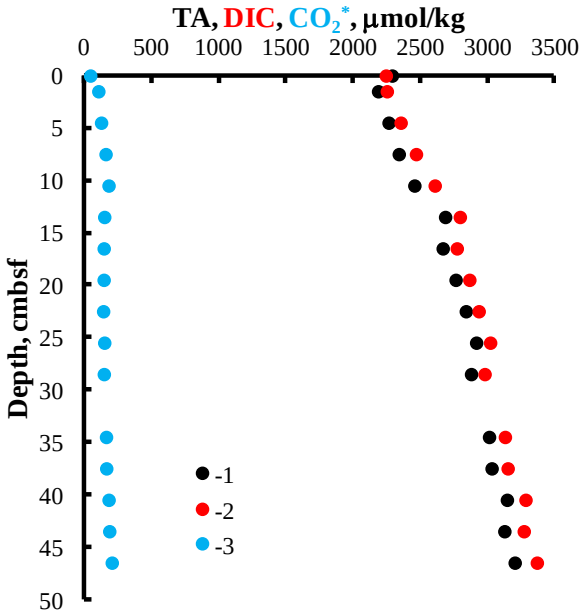

Figure 8. Vertical profiles of TA (1), DIC (2) and CO_2* (3), µmol/kg. CR41 station.

The effect of the composition of the ionic medium on the stoichiometric constants of carbonic acid and carbonate minerals is an important issue for accurate calculations of the carbonate system in porewaters. This effect can be taken into account by empirical equations relating the values of the stoichiometric constants to the prevailing salinity [55,56]. Such a simplification is possible because concentrations of the major constituents of seawater exhibit almost constant ratios to one another throughout the oceans [52]. However, relative concentrations of the major constituents are widely variable in the porewaters of marine sediments due to the early diagenesis of organic matter, which occurs in these often anoxic environments (sulfate reduction, mineral dissolution, and precipitation). Therefore, the dissociation constants obtained in seawater cannot be applied for the description of the carbonate system in anoxic marine sediments and other seawater environments with anomalous major ion concentrations, as was noted elsewhere [74,75]. In our case, the studied sediment cores were not long; therefore, the chemical anomalies of the major constituents of the porewater were not large. Nevertheless, we took into account the effect of the variability of major ion concentrations on dissociation constants using the Pitzer method [49,50]. Using the available Pitzer's parameters, the empirical relationships were developed for estimation variations in pK_{1c}, pK_2, and sp, caused by variations in the major ion concentrations (Equation (S22)–(S27); Supplemental Material). The order of variability of calcium concentrations in our case is approximately 0.2 mmol/kg (Table S1). This anomaly according to Equations (S22)–(S24) results in ΔpK_1, ΔpK_2, and Δsp as 0.00025, 0.0068, and 0.01, respectively at t = 0 °C, S = 34 psu. The maximum variation in hydrocarbonate and sulfate anion concentrations in the porewaters were 2 mmol/kg and 1 mmol/kg, respectively (Figure 7; Equation (S15)). These anomalies provide uncertainties in ΔpK_1, ΔpK_2, and Δsp of 0.0014, 0.0047, and 0.0004, respectively at t = 0 °C, S = 34 psu. These uncertainties are less than the experimental errors of the equilibrium constants and can be neglected.

5. Summary and Concluding Remarks

We found a temporal variability in the JES seawater regarding the calcite saturation degree depths of 1140 m and 960 m in 1999 and 2010, respectively. Adopting calcite saturation degrees of 91% and 80% for the lysocline and CCD, respectively, the lysocline depths decreased from 1500 m in 1999 to 1360 m in 2010, and the CCD depths also decreased from 2100 m in 1999 to 1980 m in 2010. This result suggests that the acidification of the interior of the JES occurred and that the sediments lost solid calcium carbonate over time. A comparison of the carbonate system in the seawaters and porewaters from the five stations located in the eastern part of the JES showed a sharp decrease in the pH by 0.3–0.4 pH units in the subsurface horizons (0–10 cm) compared to the pH of the seawaters of the bottom horizons. The TA in the porewaters was significantly higher than that in the overlying seawater. The anaerobic degradation of the organic matter is likely the main cause of the increasing TA in the sediments. The porewaters were significantly undersaturated with calcite, except for those from the CR34 core station, where the sediments below 7.5 cm were saturated, and even supersaturated, with calcite and aragonite. A linear correlation was found between the DIC and the TA in the sediments with a slope of 0.9993. The pH of the sediments was near-constant below 10 cm. This result suggests that there are complicated diagenetic reactions that work as a pH-stat during the anaerobic oxidation of organic matter when the sediments are located below the CCD horizon.

The diagenesis of organic matter in the top sediments of the JES forms gradients of TA and CO_2* concentration on the interface of "bottom water–sediments". The averaged fluxes of TA and DIC from sediments to bottom waters estimated by means of Fickian diffusion were 44 and 89 mmol/(m^2 year) for TA and CO_2*, respectively. If additional TA and CO_2 concentrations come up from the sediments into the bottom waters and mix within 10 meters, the increments in the TA and DIC will be 4.4 and 8.9 µmol/kg each year, respectively. Such an increment will give a drop pH of 0.016 pH unit within 10 meters of the bottom waters.

Supplementary Materials: The following are available online at https://www.mdpi.com/article/10.3390/jmse10030438/s1. Table S1: Calcium (mmol/kg) and ammonium (uM) in porewater of sediments of the JES, obtained on a board of R/V Hakuho Maru at June–July 2010; Table S2: Phosphorus and silica modeled concentrations (uM) in porewater of sediments of JES, obtained on a board of R/V Hakuho Maru at June–July 2010; Theoretical part: "Taking into account effect of variability of major ions on dissociation constants". For more details, please see [76–99]; Figure S1: Effect of sulfate reduction (decreasing sulfate concentrations and increasing carbonate alkalinity) on the stability constants of the carbonate system in seawater (salinity = 35). Symbols indicate changes in the logarithm of the first dissociation constant (**1**,**3**) and the second dissociation constant (**2**,**4**) at 25 °C and 0 °C, respectively; **5**—changes in log(K_S) at 0 °C; Figure S2: Effect of carbonate precipitation (decreasing calcium, magnesium, and carbonate alkalinity) on the stability constants of the carbonate system in seawater (salinity = 35, temperature = 0 °C). Symbols indicate changes in the logarithm of the first (**1**) and the second (**2**) dissociation constants and solubility of calcium carbonate (**3**); Table S3: The composition of seawater at S = 35; Table S4: References of Pitzer parameters which take into account interactions between cations and anions for individual electrolyte solutions used in the modeling calculations; Table S5: References of Pitzer parameters which take into account interactions in ternary electrolyte solutions (i, j, k—peces) used in the modeling calculations.

Author Contributions: Writing—original draft preparation and calculation of carbonate system parameters: P.T. (Pavel Tishchenko); synthesis and overall coordination, including retrieving sediment cores: J.Z.; TA measurements in seawater and porewater: G.P. and M.S.; pH measurements in seawater and sediments, and obtaining porewaters: P.T. (Petr Tishchenko) and S.S. All authors have read and agreed to the published version of the manuscript.

Funding: This study was partly supported by the Russian Foundation for Basic Research (No 21-55-53015-GFEN and 20-05-00381-a) and Fundamental Programs of POI—121-21500052-9 and 121021700346-7.

Institutional Review Board Statement: This study did not involve humans or animals.

Informed Consent Statement: This study did not involve humans.

Data Availability Statement: Data are available in the Supplementary Materials.

Acknowledgments: We would like to thank all the Japanese researchers and students who participated in the international cruise as well as the Captain and crews of the R/V Hakuho Maru for assistance with deck operations and shipboard sampling. We would like to thank Vyacheslav Lobanov, who put much effort for successful scientific collaboration between Russia and Japan.

Conflicts of Interest: We declare no competing interests.

References

1. Feely, R.A.; Sabine, C.L.; Lee, K.; Berelson, W.; Kleypas, J.; Fabry, V.J.; Millero, F.J. Impact of Anthropogenic CO_2 on the $CaCO_3$ System in the Oceans. *Science* **2004**, *305*, 362–366. [CrossRef]
2. Sabine, C.L.; Feely, R.A.; Gruber, N.; Key, R.M.; Lee, K.; Bullister, J.L.; Wanninkhof, R.; Wong, C.S.; Wallace, D.W.R.; Tilbrook, B.; et al. The Oceanic Sink for Anthropogenic CO_2. *Science* **2004**, *305*, 367–371. [CrossRef] [PubMed]
3. Doney, S.C.; Fabry, V.J.; Feely, R.A.; Kleypas, J.A. Ocean Acidification: The Other CO_2 Problem. *Annu. Rev. Mar. Sci.* **2009**, *1*, 169–192. [CrossRef] [PubMed]
4. Orr, J.C.; Caldeira, K.; Fabry, V.; Gattuso, J.-P.; Haugen, P.; Lehodey, P.; Pantoja, S.; Pörtner, H.-O.; Riebesell, U.; Trull, T.; et al. Research Priorities for Understanding Ocean Acidification: Summary from the Second Symposium on the Ocean in a High-CO_2 World. *Oceanography* **2009**, *22*, 182–189. [CrossRef]
5. Doney, S.C. The Growing Human Footprint on Coastal and Open-Ocean Biogeochemistry. *Science* **2010**, *328*, 1512–1516. [CrossRef]
6. Cai, W.-J.; Hu, X.; Huang, W.-J.; Murrell, M.C.; Lehrter, J.C.; Lohrenz, S.E.; Chou, W.-C.; Zhai, W.-D.; Hollibaugh, J.T.; Wang, Y.; et al. Acidification of subsurface coastal waters enhanced by eutrophication. *Nat. Geosci.* **2011**, *4*, 766–770. [CrossRef]
7. Kim, T.-W.; Lee, K.; Feely, R.A.; Sabine, C.L.; Chen, C.-T.A.; Jeong, H.J.; Kim, K.Y. Prediction of Sea of Japan (East Sea) acidification over the past 40 years using a multiparameter regression model. *Glob. Biogeochem. Cycles* **2010**, *24*, GB3005. [CrossRef]
8. Kim, J.-Y.; Kang, D.-J.; Lee, T.; Kim, K.-R. Long-term trend of CO2 and ocean acidification in the surface water of the Ulleung Basin, the East/Japan Sea inferred from the underway observational data. *Biogeosciences* **2014**, *11*, 2443–2454. [CrossRef]
9. Chen, C.-T.A.; Lui, H.-K.; Hsieh, C.-H.; Yanagi, T.; Kosugi, N.; Ishii, M.; Gong, G.-C. Deep oceans may acidify faster than anticipated due to global warming. *Nat. Clim. Chang.* **2017**, *7*, 890–894. [CrossRef]
10. Tishchenko, P.Y.; Lobanov, V.B.; Zvalinsky, V.I.; Sergeev, A.F.; Koltunov, A.; Mikhailik, T.A.; Tishchenko, P.P.; Shvetsova, M.G.; Sagalaev, S.; Volkova, T. Seasonal Hypoxia of Amursky Bay in the Japan Sea: Formation and Destruction. *Terr. Atmosp. Ocean. Sci.* **2013**, *24*, 1033–1050. [CrossRef]
11. Tishchenko, P.Y.; Tishchenko, P.P.; Lobanov, V.B.; Mikhaylik, T.A.; Sergeev, A.F.; Semkin, P.Y.; Shvetsova, M.G. Impact of the transboundary Razdolnaya and Tumannaya Rivers on deoxygenation of the Peter the Great Bay (Sea of Japan). *Estuar. Coast. Shelf Sci.* **2020**, *239*, 106731. [CrossRef]
12. Kim, I.-N.; Lee, K.; Gruber, N.; Karl, D.M.; Bullister, J.L.; Yang, S.; Kim, T.-W. Increasing anthropogenic nitrogen in the North Pacific Ocean. *Science* **2014**, *346*, 1102–1106. [CrossRef]
13. Tishchenko, P.; Lobanov, V.; Kaplunenko, D.; Sagalaev, S.; Tishchenko, P. Acidification and Deoxygenation of the Northwestern Japan/East Sea. *J. Mar. Sci. Eng.* **2021**, *9*, 953. [CrossRef]
14. Li, L.; Chen, B.; Luo, Y.; Xia, J.; Qi, D. Factors controlling acidification in intermediate and deep/bottom layers of the Japan/East Sea. *J. Geophys. Res. Oceans* **2022**, *127*, e2021JC017712. [CrossRef]
15. Chen, C.-T.A.; Wang, S.-L.; Bychkov, A.S. Carbonate chemistry of the Sea of Japan. *J. Geophys. Res. Oceans.* **1995**, *100*, 13737–13745. [CrossRef]
16. Oh, D.-C.; Park, M.-K.; Choi, S.-H.; Kang, D.-J.; Park, S.Y.; Hwang, J.S.; Andreev, A.; Hong, G.H.; Kim, K.-R. The Air-Sea Exchange of CO2 in the East Sea (Japan Sea). *J. Oceanogr.* **1999**, *55*, 157–169. [CrossRef]
17. Talley, L.D.; Tishchenko, P.; Luchin, V.; Nedashkovskiy, A.; Sagalaev, S.; Kang, D.-J.; Warner, M.J.; Min, D.-H. Atlas of Japan (East) Sea hydrographic properties in summer, 1999. *Prog. Oceanogr.* **2004**, *61*, 277–348. [CrossRef]
18. Park, G.-H.; Lee, K.; Tishchenko, P.; Min, D.-H.; Warner, M.J.; Talley, L.D.; Kang, D.-J.; Kim, K.-R. Large accumulation of antropogenic CO_2 in the East (Japan) Sea and its significant impact on carbonate chemistry. *Glob. Geochem. Cycles* **2006**, *20*, GB4013. [CrossRef]
19. Park, G.-H.; Lee, K.; Tishchenko, P. Sudden, considerable reduction in recent uptake of anthropogenic CO_2 by the East/Japan Sea. *Geophys. Res. Lett.* **2008**, *35*, L23611. [CrossRef]
20. Tishchenko, P.Y.; Pavlova, G.Y.; Shkirnikova, E.M. A new look at the alkalinity of the Sea of Japan. *Oceanology* **2012**, *52*, 21–33. [CrossRef]
21. Chang, K.-I.; Zhang, C.-I.; Park, C.; Kang, D.-J.; Ju, S.-J.; Lee, S.-H.; Wimbush, M. (Eds.) *Oceanography of the East Sea (Japan Sea)*; Springer: Cham, Switzerland; Berlin/Heidelberg, Germany; New York, NY, USA; Dordrecht, Germany; London, UK, 2016; 460p.
22. Christian, J.R.; Ono, T. (Eds.) *Ocean Acidification and Deoxygenation in the North Pacific Ocean*; PICES Special Publication: Sidney, BC, Canada, 2019; Volume 5, 116p.
23. Chen, T.-A.; Chen, X.G. *Changing Asia-Pacific Marginal Seas*; Springer Nature: Singapore, 2020; 320p.

24. Tishchenko, P.Y.; Talley, L.D.; Lobanov, V.B.; Nedashkovskii, A.P.; Pavlova, G.Y.; Sagalaev, S.G. The influence of geochemical processes in the near-bottom layer on the hydrochemical characteristics of the waters of the Sea of Japan. *Oceanology* **2007**, *47*, 350–359. [CrossRef]
25. Tamaki, K.; Pisciotto, K.; Allan, J. (Eds.) *Background, Objectives, and Principal Results, ODP Leg 127, Japan Sea; Proc. ODP, Init. Repts.*; Ocean Drilling Program: College Station, TX, USA, 1990; Volume 127, pp. 5–33. [CrossRef]
26. Ingle, J.C., Jr.; Suyehiro, K.; von Breymann, M.T. (Eds.) *Shipboard Scientific Party. Introduction, Background, and Principal Results of Leg 128 of the Ocean Drilling Program, Japan Sea; Proc. ODP, Init. Repts.*; Ocean Drilling Program: College Station, TX, USA, 1990; Volume 128, pp. 5–38. [CrossRef]
27. Hong, W.-L.; Torres, M.E.; Kim, J.-H.; Choi, J.; Bahk, J.-J. Carbon cycling within the sulfate-methane-transition-zone in marine sediments from the Ulleung Basin. *Biogeochemistry* **2013**, *115*, 129–148. [CrossRef]
28. Emerson, S.R.; Archer, D. Calcium carbonate preservation in the ocean. *Philos. Trans. R. Soc. Lond.* **1990**, *331*, 29–40. [CrossRef]
29. Broecker, W.S. The Oceanic $CaCO_3$ Cycle. *Treatise Geochem.* **2003**, *6*, 529–549.
30. Murray, J.W.; Emerson, S.; Jahnke, R. Carbonate saturation and the effect of pressure on the alkalinity of interstitial waters from the Guatemala Basin. *Geochim. Cosmochim. Acta* **1980**, *44*, 963–972. [CrossRef]
31. Archer, D.; Emerson, S.; Reimers, C. Dissolution of calcite in deep-sea sediments: pH and O_2 microelectrode results. *Geochim. Cosmochim. Acta* **1989**, *53*, 2831–2845. [CrossRef]
32. Cai, W.-J.; Reimers, C.E. The development of pH and pCO_2 microelectrodes for studying the carbonate chemistry of pore waters near the sediment-water interface. *Limnol. Oceanogr.* **1993**, *38*, 1762–1773. [CrossRef]
33. Berner, R.A.; Scott, M.R.; Thomlinson, C. Carbonate alkalinity in the pore waters of anoxic marine sediments. *Limnol. Oceanogr.* **1970**, *15*, 544–549. [CrossRef]
34. Gieskis, J.M.; Rogers, W.C. Alkalinity determination in interstitial waters. *J. Sed. Res.* **1973**, *43*, 272–277.
35. Morse, J.W. The carbonate chemistry of North Atlantic Ocean deep-sea sediment pore water. In *The Fate of Fossil Fuel CO_2 in the Oceans*; Andersen, N.R., Malakhoff, A., Eds.; Plenum Press: New York, NY, USA; London, UK, 1977; pp. 323–343.
36. Shao, C.; Sui, Y.; Tang, D.; Legendre, L. Spatial variability of surface-sediment porewater pH and related water-column characteristics in deep waters of the northern South China Sea. *Prog. Oceanogr.* **2016**, *149*, 134–144. [CrossRef]
37. Talley, L.; Min, D.H.; Lobanov, V.; Luchin, V.B.; Ponomarev, V.I.; Salyuk, A.N.; Shcherbina, A.; Tishchenko, P.; Zhabin, I. Japan/East Sea Water Masses and their Relation to the Sea's Circulation. *Oceanography* **2006**, *19*, 33–49. [CrossRef]
38. Konovalova, G.V.; Orlova, T.Y.; Pautova, L.A. *Atlas of Phytoplankton of the Sea of Japan*; Nauka: Leningrad, Russia, 1989; p. 160. (In Russian)
39. Ashjian, C.J.; Davis, C.S.; Gallager, S.M.; Alatalo, P. Characterization of the Zooplankton Community, Size Composition, and Distribution in Relation to Hydrography in the Japan/East Sea. *Deep Sea Res. Part II Top. Stud. Oceanogr.* **2005**, *52*, 1363–1392. [CrossRef]
40. Repechka, M.A. The recent Japan Sea bottom deposits. In *Problems in Geology of the Seafloor of the Japan Sea*; Academy USSR, Far Eastern Scientific Centre: Vladivostok, Russia, 1973; pp. 66–90. (In Russian)
41. Niino, H.; Emery, K.O.; Kim, C.M. Organic carbon in sediments of Japan Sea. *J. Sed. Res.* **1969**, *39*, 1390–1398.
42. Tsunogai, S.; Nishimura, M.; Nakaya, S. Complexometric titration of calcium in the presence of larger amounts of magnesium. *Talanta* **1968**, *15*, 385–390. [CrossRef]
43. Grasshoff, K.; Ehrhardt, M.; Kremling, K. (Eds.) *Methods of Seawater Analysis*, 2nd ed.; Chemie: Weinheim, Germany; Deerfield Beach, FL, USA; Basel, Switzerland, 1983; pp. 150–157.
44. Pavlova, G.Y.; Tishchenko, P.Y.; Volkova, T.I.; Dickson, A.; Wallmann, K. The intercalibration of measurement techniques for total alkalinity in seawater. *Oceanology* **2008**, *48*, 460–465. [CrossRef]
45. Wallmann, K.; Aloisi, G.; Haeckel, M.; Obzhirov, A.; Pavlova, G.; Tishchenko, P. Kinetics of organic matter degradation, microbial methane generation, and gas hydrate formation in anoxic marine sediments. *Geochim. Cosmochim. Acta* **2006**, *70*, 3905–3927. [CrossRef]
46. Dickson, A.G.; Afghan, J.D.; Anderson, G.C. Reference materials for oceanic CO_2 analysis: A method for the certification of total alkalinity. *Mar. Chem.* **2003**, *80*, 185–197. [CrossRef]
47. Tishchenko, P.Y.; Wong, C.S.; Pavlova, G.Y.; Johnson, W.K.; Kang, D.-J.; Kim, K.-R. pH measurements of seawater by means of cell without liquid Junction. *Oceanology* **2001**, *41*, 849–859.
48. Tishchenko, P.Y.; Kang, D.-J.; Chichkin, R.V.; Lazaryuk, A.Y.; Wong, C.S.; Johnson, W.K. Application of potentiometric method using a cell without liquid junction to underway pH measurements in surface seawater. *Deep Sea Res. Part I Oceanogr. Res. Pap.* **2011**, *58*, 778–786. [CrossRef]
49. Pitzer, K.S. Theory: Ion interaction approach. In *Activity Coefficients in Electrolyte Solutions*; Pytkowicz, R.M., Ed.; CRC Press: Boca Raton, FL, USA, 1979; Volume 1, pp. 157–208.
50. Pitzer, K.S. Ionic interaction approach: Theory and data correlation. In *Activity Coefficients in Electrolyte Solutions*, 2nd ed.; Pitzer, K.S., Ed.; CRC Press: Roca Raton, FL, USA; Ann Arbor, MI, USA; Boston, MA, USA; London, UK, 1991; pp. 75–153.
51. Dickson, A.G. pH buffers for sea water media based on the total hydrogen ion concentration scale. *Deep Sea Res. Part I Oceanogr. Res. Pap.* **1993**, *40*, 107–118. [CrossRef]
52. Clegg, S.L.; Whitfield, M. Activity coefficients in natural waters. In *Activity Coefficients in Electrolyte Solutions*; CRC Press: Roca Raton, FL, USA; Ann Arbor, MI, USA; Boston, MA, USA; London, UK, 1991; pp. 279–434.

53. Dickson, A. An exact definition of total alkalinity and a procedure for the estimation of alkalinity and total inorganic carbon from titration data. *Deep Sea Res. Part A. Oceanogr. Res. Pap.* **1981**, *28*, 609–623. [CrossRef]
54. Ben-Yaakov, S. A method for calculating the in situ pH of seawater. *Limnol. Oceanogr.* **1970**, *15*, 326–328. [CrossRef]
55. Millero, F.J. Thermodynamics of the carbon dioxide system in the oceans. *Geochim. Cosmochim. Acta* **1995**, *59*, 661–677. [CrossRef]
56. Dickson, A.G.; Sabine, C.L.; Christian, J.R. (Eds.) *Guide to Best Practices for Ocean CO_2 Measurements*; PICES Special Publication: Sidney, BC, Canada, 2007; Volume 3, p. 191.
57. Sarmiento, J.L.; Gruber, N. *Ocean Biogeochemical Dynamics*; Princeton University Press: Princeton, NJ, USA, 2013.
58. Brewer, P.; Wong, G.; Bacon, M.; Spencer, D.W. An oceanic calcium problem? *Earth Planet. Sci. Lett.* **1975**, *26*, 81–87. [CrossRef]
59. Redfield, A.C.; Ketchum, B.H.; Richards, F.A. The influence of organisms on the composition of sea-water. In *The Composition of Seawater: Comparative and Descriptive Oceanography*; Hill, M.N., Ed.; The Sea Interscience: New York, NY, USA, 1963; Volume 2, pp. 26–77.
60. Lobanov, V.B.; Ponomarev, V.I.; Salyuk, A.N.; Tishchenko, P.Y.; Talley, L.D. Structure and dynamics of synoptic scale eddies in the northern Japan Sea. In *Far Eastern Seas of Russia*; Oceanographic Research; Nauka: Moscow, Russia, 2007; Volume 1, pp. 450–473. (In Russian)
61. Gamo, T.; Nozaki, Y.; Sakai, H.; Nakai, T.; Tsubota, H. Spatial and temporal variations of water characteristics in the Japan Sea bottom layers. *J. Mar. Res.* **1986**, *44*, 781–793. [CrossRef]
62. Chen, C.T.A.; Feely, R.A.; Gendron, J.F. Lysocline, Calcium Carbonate Compensation Depth and Calcareou Sediments in the North Pacific Ocean. *Pac. Sci.* **1988**, *42*, 237–252.
63. Ichikura, M.; Ujiie, H. Lithology and planktonic foraminifera of the Sea of Japan piston cores. *Bull. Nat. Sci. Mus. Ser. C* **1976**, *2*, 151–182.
64. Cha, H.J. Distribution of chemical elements in sediments. In *Oceanography of the East Sea (Japan Sea)*; Springer: Berlin/Heidelberg, Germany, 2016; Chapter 9, pp. 201–215.
65. Brzezinski, M.A. The Si:C:N ratio of marine diatoms: Interspecific variability and the effect of some environmental variables. *J. Phycol.* **1985**, *21*, 347–357. [CrossRef]
66. Froelich, P.N.; Klinkhammer, G.P.; Bender, M.L.; Luedtke, N.A.; Heath, G.R.; Cullen, D.; Dauphin, P.; Hammond, D.; Hartman, B.; Maynard, V. Early oxidation of organic matter in pelagic sediments of the eastern equatorial Atlantic: Suhoxic dia-genesis. *Geochim. Cosmochim. Acta* **1979**, *43*, 1075–1090. [CrossRef]
67. Emerson, S.; Jahnke, R.; Bender, M.; Froelich, P.; Klinkhammer, G.; Bowser, C.; Setlock, G. Earley diagenesis in sediments from the Eastern Equatorial Pacific. I. Pore water nutrient and carbonate results. *Earth Planet. Sci. Lett.* **1980**, *49*, 57–80. [CrossRef]
68. Middelburg, J.J.; Levin, L.A. Coastal hypoxia and sediment biogeochemistry. *Biogeosciences* **2009**, *6*, 1273–1293. [CrossRef]
69. Boudreau, B.P.; E Canfield, D. A comparison of closed- and open-system models for porewater pH and calcite-saturation state. *Geochim. Cosmochim. Acta* **1993**, *57*, 317–334. [CrossRef]
70. Gazeau, F.; van Rijswijk, P.; Pozzato, L.; Middelburg, J.J. Impacts of Ocean Acidification on Sediment Processes in Shallow Waters of the Arctic Ocean. *PLoS ONE* **2014**, *9*, e94068. [CrossRef] [PubMed]
71. Rassmann, J.; Lansard, B.; Gazeau, F.; Guidi-Guilvard, L.; Pozzato, L.; Alliouane, S.; Grenz, C.; Rabouille, C. Impact of ocean acidification on the biogeochemistry and meiofaunal assemblage of carbonate-rich sediments: Results from core incubations (Bay of Villefranche, NW Mediterranean Sea). *Mar. Chem.* **2018**, *203*, 102–119. [CrossRef]
72. Berner, R.A. *Early Diagenesis. A Theoretical Approach*; Princeton University Press: Princeton, NJ, USA, 1980; p. 241.
73. Schults, H.D. Quantification of Early Diagenesis: Dissolved Constituents in Marine Pore Water. In *Marine Geochemistry*, 2nd ed.; Horst, D., Schulz, M.Z., Eds.; Springer: Berlin/Heidelberg, Germany; New York, NY, USA, 2006; pp. 75–124.
74. Ben-Yaakov, S.; Goldhaber, M.B. The influence of sea water composition on the apparant constants of the carbonate system. *Deep. Sea Res. Oceanogr. Abstr.* **1973**, *20*, 87–99. [CrossRef]
75. Pytkowicz, R.M. Activity coefficients of bicarbonates and carbonates in seawater. *Lymnol. Oceanogr.* **1975**, *20*, 971–975. [CrossRef]
76. Dickson, A.G.; Millero, F.J. A comparison of the equilibrium constants for the dissociation of carbonic acid in seawater media. *Deep-Sea Res.* **1987**, *34*, 1733–1743. [CrossRef]
77. Harvie, C.E.; Moller, N.; Weare, J.H. The prediction of mineral solubilities in natural waters: The Na-K-Mg-Ca-H-Cl-SO_4-OH-HCO_3-CO_3-CO_2-H_2O system to high ionic strengths at 25 °C. *Geochim. Cosmochim. Acta* **1984**, *48*, 723–751. [CrossRef]
78. Pabalan, R.T.; Pitzer, K.S. Thermodynamics of concentrated electrolyte mixtures and the prediction of mineral solubilities to high temperatures in the Na-K-Mg-Cl-SO_4-OH-H_2O. *Geochim. Cosmochim. Acta* **1987**, *51*, 2429–2443. [CrossRef]
79. Millero, F.J.; Pierrot, D. A chemical model for natural waters. *Aquatic Geochem.* **1998**, *4*, 153–199. [CrossRef]
80. Pitzer, K.S. Thermodynamics of electrolytes. I Theoretical basis and general equation. *J. Phys. Chem.* **1973**, *77*, 268–277. [CrossRef]
81. Whitfield, M. The extension of chemical models for sea water to include trace components at 25 C and 1 atm pressure. *Geochim. Cosmochim. Acta* **1975**, *39*, 1545–1557. [CrossRef]
82. Pitzer, K.S.; Silvester, L.F. Thermodynamics of electrolytes. VI. Weak electrolytes including H_3PO_4. *J. Soln. Chem.* **1976**, *5*, 269–278. [CrossRef]
83. Plummer, L.N.; Busenberg, E. The solubility of calcite, aragonite and vaterite in CO_2-H2O solutions between 0 and 90 C, and an evaluation of the aqueous model for the system $CaCO_3$-CO_2-H_2O. *Geochim. Cosmochim. Acta* **1982**, *46*, 1011–1040. [CrossRef]
84. Drever, J.I. The magnesium problem. In *The Sea*; Goldberg, E.D., Ed.; John Wiley & Sons: New York, NY, USA; London, UK; Sydney, Austalia; Toronto, ON, Canada, 1974; Volume 5, pp. 337–357.

85. Gieskes, J.M. The chemistry of interstitial waters of deep sea sediments: Interpretation of deep sea drilling data. In *Chemical Oceanography*; Riley, J.P., Chester, R., Eds.; Academic Press: London, UK; New York, NY, USA, 1983; Volume 8, pp. 222–269.
86. Aloisi, G.; Wallmann, K.; Bollwerk, S.M.; Derkachev, A.; Bohrmann, G.; Suess, E. The effect of dissolved barium on biogeochemical processes at cold seeps. *Geochim. Cosmochim. Acta* **2004**, *68*, 1735–1748. [CrossRef]
87. Pitzer, K.S.; Peiper, J.C.; Busey, R.H. Thermodynamic properties of aqueous sodium chloride solutions. *J. Phys. Chem. Ref. Data* **1984**, *13*, 1–102. [CrossRef]
88. Peiper, J.C.; Pitzer, K.S. Thermodynamics aqueous carbonate solutions including mixtures of sodium carbonate, bicarbonate and chloride. *J. Chem. Thermodyn.* **1982**, *14*, 613–638. [CrossRef]
89. Marion, G.M. Carbonate mineral solubility at low temperatures in the Na-K-Mg-Ca-Cl-H-SO_4-OH-HCO_3-CO_3-CO_2-H_2O system. *Geochim. Cosmochim. Acta* **2001**, *65*, 1883–1896. [CrossRef]
90. De Lima, M.C.P.; Pitzer, K.S. Thermodynamics of saturated electrolyte mixtures of NaCl with Na_2SO_4 and $MgCl_2$. *J. Soln. Chem.* **1983**, *12*, 187–201. [CrossRef]
91. Phutela, R.C.; Pitzer, K.S. Heat capacity and other thermodynamic properties of aqueous magnesium sulfates. *J. Phys. Chem.* **1986**, *90*, 895–901. [CrossRef]
92. Pitzer, K.S.; Olsen, J.; Simonson, J.M.; Roy, R.N.; Gibbons, J.J.; Rowe, L. Thermodynamics of magnesium and calcium bicarbonates and mixtures with chloride. *J. Chem. Eng. Data* **1985**, *30*, 14–17. [CrossRef]
93. Holmes, H.F.; Mesmer, R.E. Thermodynamic properties of aqueous solutions of the alkali metal chlorides to 250 °C. *J. Phys. Chem.* **1983**, *87*, 1242–1254. [CrossRef]
94. Holmes, H.F.; Mesmer, R.E. Thermodynamics of aqueous solutions of the alkali metal sulfates. *J. Soln. Chem.* **1986**, *15*, 495–518. [CrossRef]
95. Roy, R.N.; Gibbons, J.J.; Wood, M.D.; Williams, R.W. The first ionization of carbonic acid in aqueous solutions of potassium chloride including the activity coefficients of potassium bicarbonate. *J. Chem. Thermodyn.* **1983**, *15*, 37–47. [CrossRef]
96. Greenberg, J.P.; Moller, N. The prediction of miniral solubilities in natural waters. A chemical equilibrium model for the Na-K-Ca-SO_4-H_2O system to high concentration from 0 to 250 °C. *Geochim. Cosmochim. Acta* **1989**, *53*, 2503–2518. [CrossRef]
97. Harned, H.; Davis, R. The ionization constant of carbonic acid in water and the solubility of carbon dioxide in water and aqueous salt solutions from 0 to 50°. *J. Am. Chem. Soc.* **1943**, *65*, 2030–2037. [CrossRef]
98. He, S.; Morse, J.W. The carbonic acid system and calcite solubility in aqueous Na-K-Ca-Mg-Cl-SO_4 solutions from 0 to 90 °C. *Geochim. Cosmochim. Acta* **1993**, *57*, 3533–3554. [CrossRef]
99. Wong, C.S.; Tishchenko, P.Y.; Johnson, W.K. Solubility of Carbon Dioxide in Aqueous HCl and $NaHCO_3$ Solutions from 278 to 298 K. *J. Chem. Eng. Data* **2005**, *50*, 817–821. [CrossRef]